IOP PUBLISHING JOURNAL OF PHYSICS D: APPLIED PHYSICS

J. Phys. D: Appl. Phys. **42** (2009) 234006 (9pp) doi:10.1088/0022-3727/42/23/234006

Flexible microwave PIN diodes and switches employing transferrable single-crystal Si nanomembranes on plastic substrates

Guoxuan Qin[1,4], Hao-Chih Yuan[1,4,5], George K Celler[2], Weidong Zhou[3] and Zhenqiang Ma[1]

[1] Department of Electrical and Computer Engineering, University of Wisconsin-Madison, Madison, WI 53706, USA
[2] Soitec USA, 2 Centennial Drive, Peabody, MA 01960, USA
[3] Department of Electrical Engineering, University of Texas at Arlington, Arlington, TX 76019, USA

E-mail: mazq@engr.wisc.edu

Received 1 September 2009
Published 17 November 2009
Online at stacks.iop.org/JPhysD/42/234006

Abstract

This paper reports the realization of flexible RF/microwave PIN diodes and switches using transferrable single-crystal Si nanomembranes (SiNM) that are monolithically integrated on low-cost, flexible plastic substrates. High frequency response is obtained through the realization of low parasitic resistance achieved with heavy ion implantation before nanomembrane release and transfer. The flexible lateral SiNM PIN diodes exhibit typical rectifying characteristics with insertion loss and isolation better than 0.9 dB and 19.6 dB, respectively, from DC to 5 GHz, as well as power handling up to 22.5 dBm without gain compression. A single-pole single-throw (SPST) flexible RF switch employing shunt-series PIN diode configuration has achieved insertion loss and isolation better than 0.6 dB and 22.9 dB, respectively, from DC to 5 GHz. Furthermore, the SPST microwave switch shows performance improvement and robustness under mechanical deformation conditions. The study demonstrates the considerable potential of using properly processed transferrable SiNM for microwave passive components. Future investigations on transferrable SiNMs will lead to eventual realization of monolithic microwave integrated systems on low-cost flexible substrates.

(Some figures in this article are in colour only in the electronic version)

1. Introduction

High performance large-area microelectronics (or macroelectronics/flexible electronics) with extreme mechanical properties (e.g. bendability) have attracted increasing attention for the past decade [1]. The unique features of flexible electronics such as high flexibility, light weight, resistance to impact and capability to be conformally attached to uneven or rugged surfaces make them superb candidates for a wide variety of applications. Examples include large-area displays, electronic textiles, biomedical sensors and low-cost ICs [2–8].

A considerable number of semiconductor materials have been employed as active device materials for flexible electronics. Among them, amorphous silicon, organics and polymers and polycrystalline silicon are the most commonly used ones. These materials are suitable for most low-speed (or low-frequency) flexible electronics applications. Besides these low-speed applications, there are a number of

[4] These authors contributed equally.
[5] Present address: National Renewable Energy Lab, 1617 Cole Bovd., Golden, CO, USA.

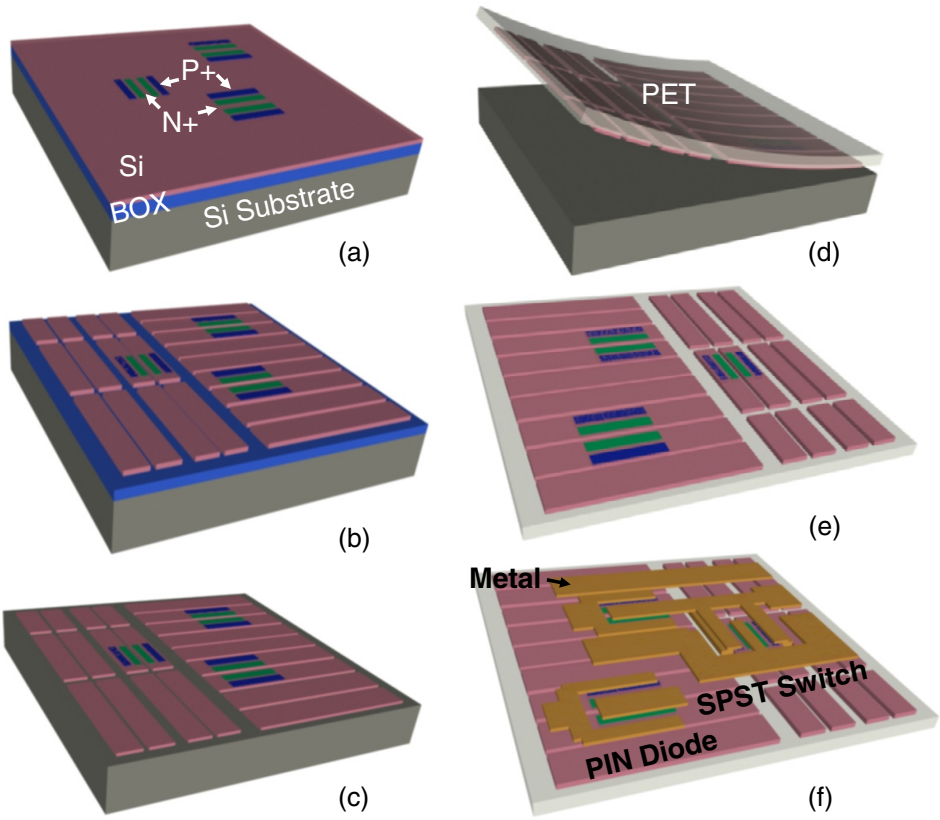

Figure 1. Fabrication process illustration for PIN diode and series-shunt PIN diode RF switches. (*a*) Beginning with SOI. P+ and N+ regions were selectively ion implanted after photolithography steps, followed by thermal annealing. (*b*) The ion implanted top Si layer was then patterned into strips. Plasma dry etching was employed to etch away the Si and expose the buried oxide layer (BOX). (*c*) The SOI was immersed into HF to release the top Si layer as SiNM. SiNM settled down and became weakly bonded with the handle substrate ('in-place bonding'). (*d*) A PET substrate with SU-8 spun on was brought face to face in contact with the Si substrate for flip transfer of SiNM. The SiNM strips were picked up by the PET substrate due to the stronger bonding force of SU-8 with SiNM, completing the flip transfer of SiNM. (*e*) The PET substrate was flipped with the original bottom side of SiNM being upside. (*f*) Metallization with e-beam metal evaporation to complete the fabrication of the PIN diodes and SPST RF switches. (Colour online).

flexible applications where high-speed and high-frequency (e.g. RF and even microwave, >1 GHz) operations are required. Examples include RFIDs, personal wireless devices (such as Wi-Fi gadgets, etc) and large area, rollable and/or foldable airborne/space-borne communication systems and surveillance and remote sensing radars [1, 6]. Unfortunately none of the traditional flexible semiconductor materials can offer the high-speed capability due to their low crystalline quality and low carrier mobilities. To fulfil these higher performance demands for flexible electronics, high-speed semiconductor materials with high carrier mobility and high saturation velocity are required. Recently developed transferrable and flexible single crystalline Si nanomembrane (SiNM), lifted from silicon-on-insulator (SOI) (see figure 1) may be the most promising. Compared with other materials that have high carrier mobility (e.g. carbon nanotubes and ZnO), it is easier to process and is more mechanically robust [9–11]. Of more importance, the high carrier mobility of SiNMs, which is as high as their rigid bulk wafer counterparts [9, 11, 12], makes them promising for very high-frequency applications.

To transform the superior carrier transport characteristics of SiNMs into high-speed thin-film transistors (TFTs), we have developed a unique combined high-temperature and low-temperature process for transferrable SiNMs [13]. The process development has led to the realization of microwave TFTs on a plastic substrate. The promise of SiNM is further demonstrated by the record TFT speed (f_{max}: 7.8 GHz with a gate length of 2.5 μm) achieved recently [14]. Further downscaling of the TFTs' critical dimensions on plastic substrates is expected to lead these flexible devices to much higher operation frequencies in the near future.

Despite the important advances on flexible microwave active devices, flexible passive components that can be monolithically integrated with these high-frequency active TFTs on the plastic substrate and are also capable of microwave frequency operation have not yet been reported. Considering that the P-intrinsic-N (PIN) diode is one of the key components in many microwave systems (e.g. switch arrays, phase shifters and limiters), we report here the fabrication and characterizations of high-performance flexible lateral PIN diodes and PIN diode RF switches made in SiNMs in this paper. The performance of the microwave switches under mechanical bending conditions is also reported in detail.

2. Device fabrication

The fabrication process of the PIN diodes and switches on a plastic substrate using the SiNM transfer technique is completely compatible with that used to fabricate flexible TFTs, as depicted previously [13]. The compatibility will considerably ease the eventual monolithic integration of active TFTs and the switches on the same flexible substrate. The process flow is illustrated in figure 1. The fabrication begins with a lightly doped p-type Si(0 0 1) UNIBOND® SOI substrate with a 200 nm Si top layer and a 200 nm buried oxide (BOX) layer. Optical photolithography was performed to define the heavily doped n- and p-type regions in the top Si layer. Two-step ion implantation was then performed for the N+ and P+ regions with the following conditions: 4×10^{15} cm^{-2} phosphorus ions at 40 keV, and 4×10^{15} cm^{-2} boron ions at 25 keV, respectively. After that, the sample was annealed at 850 °C for 45 min in ambient N_2 in a furnace (figure 1(*a*)). These processing steps gave the desired high doping concentrations in the top Si layer, which ensure low sheet resistance and low contact resistance [13] that are critical for realizing high-performance RF devices, including RF switches as described later in the text. All the processing that follows consists of low-temperature (low-T) steps. The 200 nm Si layer was then patterned into 30 μm wide strips with photolithography followed by a plasma dry etching (SF_6/O_2) down to the BOX layer (figure 1(*b*)). After stripping off the photoresist, the sample was put into hydrofluoric acid (HF) to etch away the underlying BOX layer and release the Si strips. In order to release the top Si layer, it can be patterned into many other forms. For example, the released Si layer can be patterned as a single sheet containing an array of holes. All these forms are generally called Si nanomembranes (SiNMs).

As the patterned SiNM was released, it settled down and weakly bonded with the Si handling substrate via weak van der Waals forces [15]. Due to the thinness of the BOX layer (200 nm here versus micrometre thickness in some other types of SOI), the released Si strips, in spite of being very flexible, kept their spatial registration the same as it was during the photolithography step (figure 1(*c*)). Then the sample was rinsed thoroughly with DI water and was subsequently brought *face to face* and firmly contacted with a polyethylene terephthalate (PET) substrate that was spin coated with a SU-8 epoxy layer. No intentional exposure was made to the SU-8 at this moment. Since the bonding force between the SiNM and the epoxy is stronger than the Si-to-Si bonding, the SiNM can be lifted off from the SOI substrate and *flip*-transferred onto the PET substrate (figure 1(*d*)). A UV exposure step was then used to cure the SU-8.

The flip transfer technique ensures that the position of the patterned Si strips does not change throughout the entire process so that the pre-doped regions can be further registered with the rest of the mask layers even after they were transferred onto the plastic substrate [11, 13]. As a result, higher fidelity registration of SiNMs can be easily achieved than by using any other transfer methods. However, the flip transfer requires that a thin BOX layer (roughly less than 0.5 μm) be used in order to avoid using anchors or tethers [16] to prevent position shifts of the SiNMs during their release. In addition, due to the SiNM flipping during transfer, proper ion implantation and annealing conditions are needed to ensure that high doping concentrations for both n- and p-types are realized on the *bottom* side of the Si layer before release (in order to form high-quality Ohmic contacts on the bottom surface later). The special ion implantation and annealing requirement makes thin SiNMs more suitable than very thick ones for this fabrication process.

As the next step, the PET substrate was then flipped over to expose the bottom side of the SiNM for further processing (figure 1(*e*)). Finally, metal contacts and interconnects were formed by evaporating a stack layer of 40/500 nm Cr/Au following a photolithography step (figure 1(*f*)). Both individual PIN diodes and single-pole single-throw (SPST) switches were fabricated on the same PET substrate as illustrated in figure 1(*f*). As can be seen, by combining the high-temperature (high-T, performed on SOI) and the low-T processes, we have circumvented the paradoxical challenge that plastic substrates are intolerant to high-temperature processes and that the high-temperature processes are absolutely necessary to achieve high doping concentrations and thus low parasitic resistances. In fact, the highest temperature that was applied to the plastic substrates was kept below 120 °C (applied to PET for photoresist baking), which is below the temperature tolerance (∼170 °C: Vicat softening point) of PET substrates.

Unlike conventional vertical PIN diode structures, the P-, I- and N-regions in this study were arranged laterally on the SiNM. While the thinness of the SiNM allows one to achieve desirable mechanical flexibility, the lateral arrangement of the PIN structure has eased its fabrication on the thin SiNMs. The width of the I-region is determined by the distance between the P+ and N+ regions during photolithography. An I-region width of 2 μm is used in this study in order to achieve high-frequency response while maintaining proper breakdown voltages for power handling. The diode cross-section area can be calculated by multiplying the width of the P+ (or N+) region by the thickness of the SiNM (200 nm). The fabricated diodes have various areas ranging from 80 to 320 μm^2. SPST switches configured with these PIN diodes were also fabricated on the PET substrate. Figure 2(*a*) presents a schematic cross-section of the lateral SiNM PIN diode. Figure 2(*b*) shows an optical image of the flexible PIN diodes and switch arrays on the PET substrate. Figures 2(*c*) and (*d*) show the optical-microscope images of a finished lateral SiNM PIN diode with an area of 80 μm^2 and a shunt-series SPST switch containing two PIN diodes (area of both is 40 μm^2), respectively. The insets in these two figures show the corresponding circuit diagrams of the PIN diode and SPST switch, respectively.

3. Results and discussion

3.1. Series PIN diodes

DC characteristics of the flexible SiNM PIN diodes were measured with an HP4155B semiconductor parameter

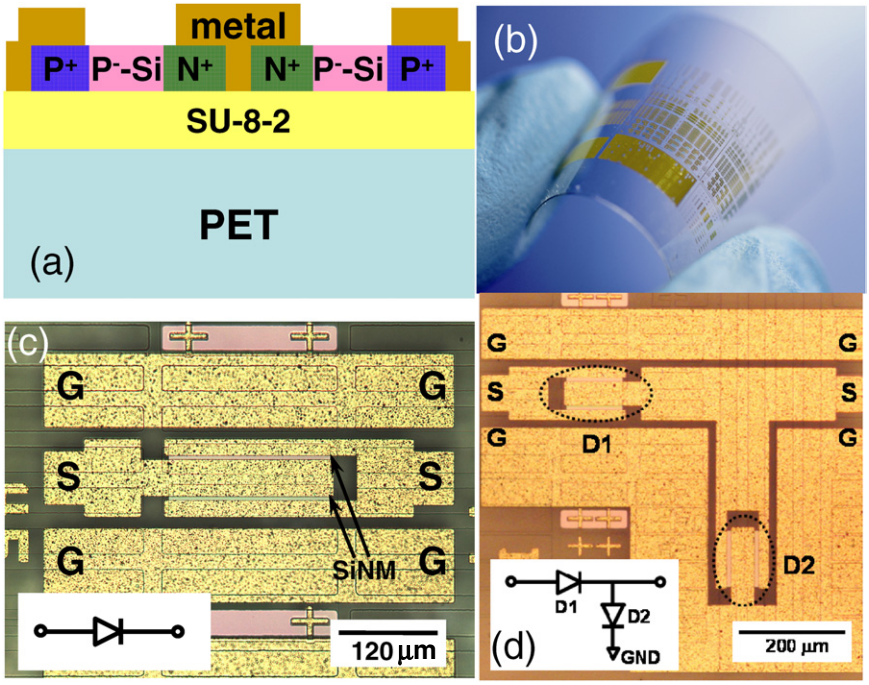

Figure 2. (*a*) Schematic cross-section of lateral SiNM PIN diodes on a flexible PET substrate. The 'I' (p^--Si) region width of all the PIN diodes is 2 μm. The SiNM thickness is 200 nm. The SU-8 layer is ∼2 μm thick. The PET substrate is ∼175 μm thick. (*b*) Optical image of finished PIN diode and switch arrays on a bent PET substrate. (*c*) Optical microscope image of a finished SiNM PIN diode. The centre metal electrodes (labelled 'S' for 'signal') cover two strips of the transferred SiNM and the length of each strip is 200 μm. The area of this PIN diode is 80 μm^2. Shown in the inset is the diode circuit diagram. (*d*) Optical microscope image of a finished shunt-series PIN diode SPST switch. The diode area of both D1 and D2 is 40 μm^2. The circuit diagram of the SPST RF switch is shown in the inset. (Colour online).

analyzer. Figure 3(*a*) shows the measured *I*–*V* curves of an 80 μm^2 SiNM PIN diode on a plastic substrate at room temperature [17]. In this figure, typical diode rectifying characteristics are observed from the flexible SiNM PIN diode on plastic. No apparent breakdown appears up to 10 V reverse bias. The ideality factor n is extracted to be 1.53. The value is possibly influenced by the high recombination rate due to the large periphery-to-area ratio that is inherent to the lateral PIN diodes [18].

RF characteristics of the PIN diodes were measured with an Agilent E8364A performance network analyzer using 100 μm pitch ground-signal-ground (GSG) probes. The reference plane was calibrated to the probe tip by short-open-load-thru (SOLT) calibration using the impedance standard substrate from DC to 40 GHz. Small-signal *S*-parameters were measured for the SiNM PIN diodes under both ON and OFF conditions [17]. To test the power handling capability of the flexible PIN diode, large-signal performance was measured using a Focus Microwaves CCMT-1816 load-pull system at 6 GHz.

Such data are shown in figure 3(*b*) for a 240 μm^2 SiNM PIN diode operating at 6 GHz, with a forward-biased current $I_f = 20$ mA. Linear dependence between P_{IN} and P_{OUT} is demonstrated for the input power ranging from 7.5 to 22.5 dBm, indicating the superior power handling capability of the flexible PIN diodes. The PIN diode suffered from irreversible burn-out at an input power of around 25 dBm. Nonetheless, no gain compression is observed on the lateral SiNM PIN diode within the measured power range. The average large-signal gain is around −1.1 dB and agrees very well with the insertion loss (0.91 dB) measured by small-signal *S*-parameters (as shown in figure 4(*a*)) at the same frequency and under the same bias condition.

Small-signal *S*-parameters of several individual series SiNM PIN diodes were measured under different forward-bias current levels (ON states) and zero bias (OFF state). To illustrate the effects of the diode size on RF characteristics, figure 4 presents and compares the measured S21 (figure 4(*a*)) and S11 (figure 4(*b*)) for two SiNM PIN diodes with different areas: 80 and 240 μm^2. In order to simplify the comparison, the same bias conditions were used for both the diodes. The ON state has three forward-biased current levels (I_f) at 10, 20 and 30 mA and the OFF state is at zero bias. The measured S21 under the ON state and the OFF state is equivalent to the insertion loss and isolation of the series PIN diodes, respectively, whereas S11 is return loss for both the ON and the OFF states. Due to the symmetrical and reciprocal nature of the single series PIN diode, the measured S12 (S22) is identical with S21 (S11) and is not plotted in the figures. As shown in figure 4(*a*), the insertion loss on both the small- (80 μm^2) and the large-area (240 μm^2) series SiNM PIN diode decreases with increasing I_f and is better than 0.94 and 0.79 dB from DC up to 20 GHz at $I_f = 30$ mA for the small- and the large-area diode, respectively. Apparently, better insertion loss can be realized with higher bias current for both diodes. Isolation higher than 19 dB is exhibited on the small-area PIN diode at zero bias in the frequency range from DC to 5 GHz. The large-area diode, however, has much lower isolation and is only better than 11.6 dB up to 5 GHz. When increased reverse voltage bias (from 1 to 8 V) was applied on the series SiNM PIN

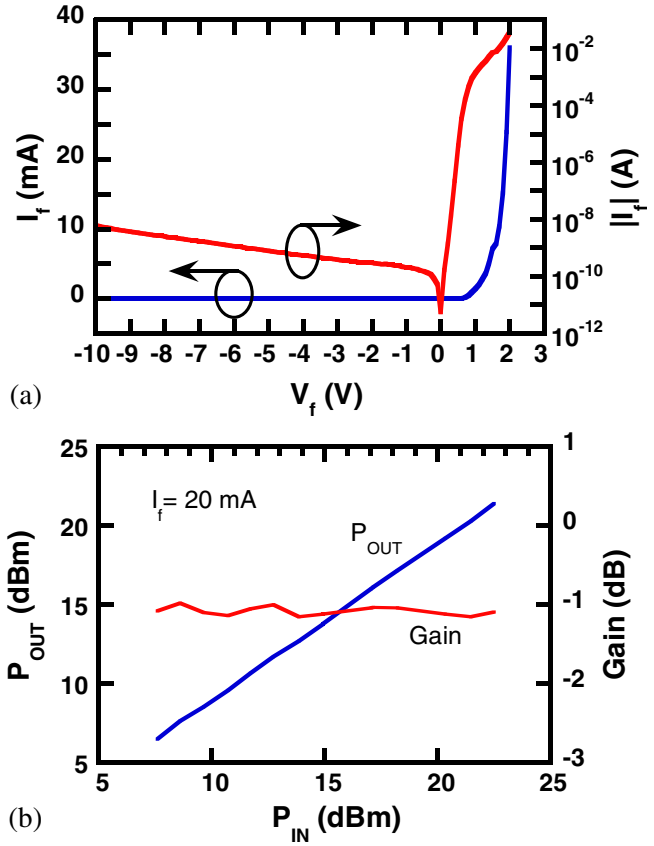

Figure 3. (*a*) Measured I–V curve of a 80 μm^2 lateral SiNM PIN diode on a flexible PET substrate. (*b*) RF power measurement results at 6 GHz of the series SiNM PIN diode biased at I_f = 20 mA. Diode area is 240 μm^2. (Colour online).

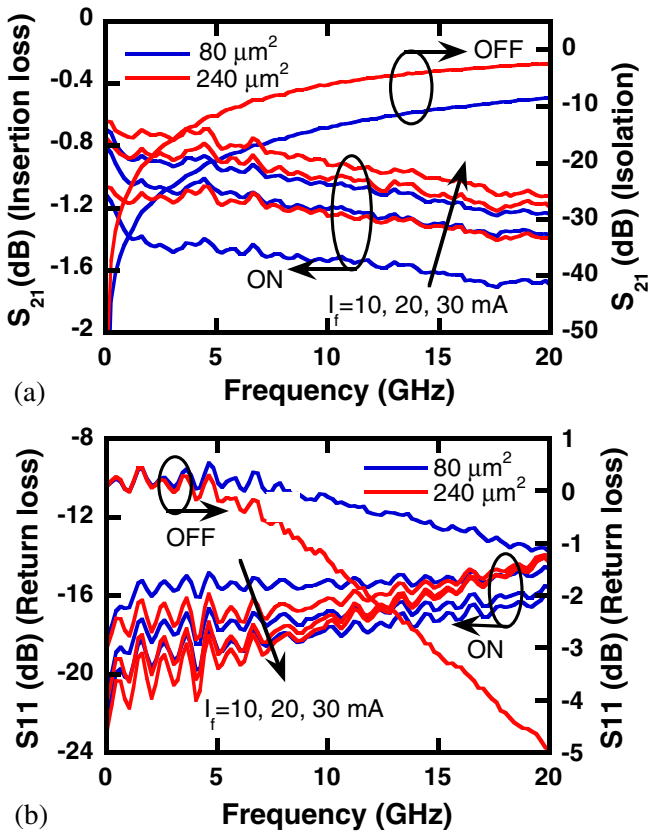

Figure 4. (*a*) Measured S21 (S12 is the same as S21, not shown) and (*b*) S11 (S22 is very close to S11, not shown) of two series SiNM PIN diodes with diode area of 80 and 240 μm^2. The ON state is biased at I_f = 10, 20 and 30 mA. The OFF state is biased at zero bias (I_f = 0 mA). (Colour online).

diodes, isolation shows negligible improvement (<1 dB). This is strong evidence that all the lateral SiNM PIN diodes in this study have fully depleted I-regions and do not require negative voltage bias to achieve the optimal isolation during operation. The return loss (S11) also improves with the increase in the forward-bias current level under the ON state, as shown in figure 4(*b*). Under the same forward-bias current level for the ON state, the small-area diode exhibits better return loss than the large-area diode in the high frequency range. The trend reverses for the OFF state. In addition, the ON-state return loss is much better than that of the OFF state, which can be easily understood.

The observed effects of diode size on the RF characteristics, as described above, are consistent with other sizes (areas) of diodes. Table 1 summarizes the RF performance characteristics of the flexible SiNM PIN diodes with all different diode areas (80–320 μm^2). All the relevant performance values are extracted from the as-measured S-parameters at a frequency of 5 GHz for easy comparison. It is clear from this table that the insertion loss improves with the increase in the diode area, however, with the penalty of degraded isolation. The return loss for the ON state slightly improves with the diode area, which is consistent with the insertion loss trend.

To better understand the performance of the flexible PIN diodes, theoretical analysis has been conducted. As shown in the previous study [19], the I-region resistance under forward-biased condition can be expressed as

$$R_i = \frac{w_i^2}{I_f \tau (\mu_n + \mu_p)}, \quad (1)$$

where w_i is the width of the I-region, I_f is the forward-biased current and τ is the effective carrier lifetime. μ_n, μ_p are the mobilities of electrons and holes, respectively. It is clear from equation (1) that the I-region resistance decreases with the increase in the forward-bias current level. As a result, the insertion loss/return loss improves with the increase in I_f. Although the R_i is independent of the diode area from equation (1), the contact resistance (R_c) and access resistance (R_s) at the heavily doped P+ and N+ regions are possibly the major factors (Note: even the best metal–semiconductor Ohmic contact has resistance) for the total resistance under forward-biased condition in this study. Therefore, larger-area SiNM PIN diodes have smaller total parasitic resistances and exhibit lower insertion loss (as shown in figure 4 and table 1). Since the metal contacts were made on the backside (i.e. the bottom side before release) of the pre-doped SiNMs after their transfer (as shown in figure 1), achieving sufficient high doping concentrations with good crystallinity on the backside was very critical in order to realize the minimized R_c and R_s. We have achieved both high doping concentration and good crystallinity with the pre-release ion implantation and thermal annealing.

Table 1. Frequency responses of the flexible series SiNM PIN diodes and shunt-series switch at 5 GHz.

Device	Insertion loss (S21) at $I_f = 30$ mA (dB)	Isolation (S21) $I_f = 0$ mA (dB)	Return loss (S11/S22) ON at $I_f = 30$ mA (dB)	Return loss (S11/S22) OFF at $I_f = 0$ mA (dB)
Series PIN diode ($A = 80\,\mu m^2$)	0.94	19.6	18.8	0.15
Series PIN diode ($A = 160\,\mu m^2$)	0.84	13.4	19.5	0.20
Series PIN diode ($A = 240\,\mu m^2$)	0.79	11.6	19.7	0.19
Series PIN diode ($A = 320\,\mu m^2$)	0.70	7.60	19.8	1.06
Shunt-series RF switch A (D1 = 240 μm^2 D2 = 40 μm^2)	0.63	$I_2 = 0$ mA 10.8 $I_2 = 10$ mA 22.9	20.5/21.1	$I_2 = 0$ mA 0.55/0.91 $I_2 = 10$ mA 0.08/7.70

The isolation of the series PIN diodes can be expressed as [20]

$$\text{Isolation} = 10 \cdot \log\left[1 + \left(\frac{x_t}{2Z_o}\right)^2\right], \qquad (2)$$

where $x_t = 1/2\pi f C_t$ and C_t is the diode junction capacitance under reverse bias. When the diode area is larger, C_t increases while x_t decreases, thus the isolation on SiNM PIN diodes becomes degraded. The trend is clearly reflected in the results shown in figure 4 and table 1.

While single series PIN diodes can also serve as an RF switch, we have clearly noticed from our measurement results and theoretical analyses that optimal insertion loss and isolation could not be obtained simultaneously by using only the series diodes. Since better insertion loss can be obtained from larger-area diodes, it is thus desirable to also achieve better isolation for the large-area PIN diodes. Such an objective can be realized by forming RF switches employing shunt-series configuration of two PIN diodes. In the following subsection, we describe the performance characteristics of such RF switches. By employing the shunt-series configuration for the RF switches, an insertion loss and isolation better than 0.6 and 22.9 dB (without mechanical bending), respectively, is obtained from DC to 5 GHz on a low-cost, flexible PET substrate, much better than that obtained from individual series PIN diodes.

3.2. Shunt-series configured switches

SPST RF switches using shunt-series configuration, with their layout shown in figures 1(*f*) and 2(*d*), were realized with identical fabrication steps as depicted previously for the series diodes. The RF performance characteristics of the switches with different diode area configurations were compared. For switch A, the areas of the series (D1) and the shunt (D2) PIN diode are 240 μm^2 and 40 μm^2, respectively. For switch B, the series (D1) and the shunt diode (D2) areas are both 40 μm^2. The ON state small-signal *S*-parameters of the two switches were characterized with forward-biased current I_f of 10, 20 30 mA applied on the input end (port 1, D1) of the switches. The OFF state responses were measured at zero bias and a forward-bias current of 10 mA (I_2) applied on the shunt PIN diode (D2).

Figure 5 shows the measured small-signal frequency response characteristics of the two shunt-series SiNM PIN SPST switches. As shown in figure 5(*a*), switch A exhibits much better insertion loss than switch B under the ON state. It is obvious that D1 dominates the ON state performance, which is consistent with the results obtained for the series diodes described earlier, i.e. the larger-area diode (D1 in switch A) has a smaller insertion loss. Figure 5(*b*) shows the return loss of the two switches under the ON state. As shown in the figure, the return loss of switch A is much better than that of switch B, consistent with what is shown in figure 5(*a*). In essence, the difference of return loss of the two switches is due to the total series resistance of the series diode (D1) being higher for switch B than for switch A. Similar to the series diodes (as shown in figure 4(*b*)), return loss S11 is almost the same as S22 for the switches.

Figure 5(*c*) shows the isolation (OFF state) of the shunt-series switch under $I_f = 0$ mA (D1 is off) and D2 bias (I_2) at 0 and 10 mA. For both switches, the isolation is considerably improved by forward biasing the shunt diode D2. The reason for the improvement is that D2 under forward bias effectively created a short path to the ground for the incident power from the output port (as shown in figure 2(*d*)). Furthermore, the isolation of switch B is better than that of switch A under the equivalent bias for D2. The differences of S21 originate from the different areas of D1 in these two switches. As indicated in equation (2), the larger is the area D1, the larger is its junction capacitance. As a result, the isolation is further degraded. Nevertheless, with the presence of D2, the isolation of the switch has been considerably improved (e.g. 22.9 dB at $I_2 = 10$ mA for switch A versus 11.6 dB at 5 GHz for diode area of 240 μm^2) in comparison with that of the series diodes alone (see table 1).

Figure 5(*d*) shows the return loss (S11 and S22) of the two switches under two bias conditions for their D2 ($I_2 = 0$ and 10 mA). As indicated in the figure, for both switches S22 is significantly improved while S11 is slightly degraded when D2 is forward biased. For both S11 and S22, switch A exhibited more improvement than switch B, indicating more effectiveness of the short path created for switch A than for switch B by D2 under its forward-bias condition. The return loss results are consistent with the isolation results shown in figure 5(*c*).

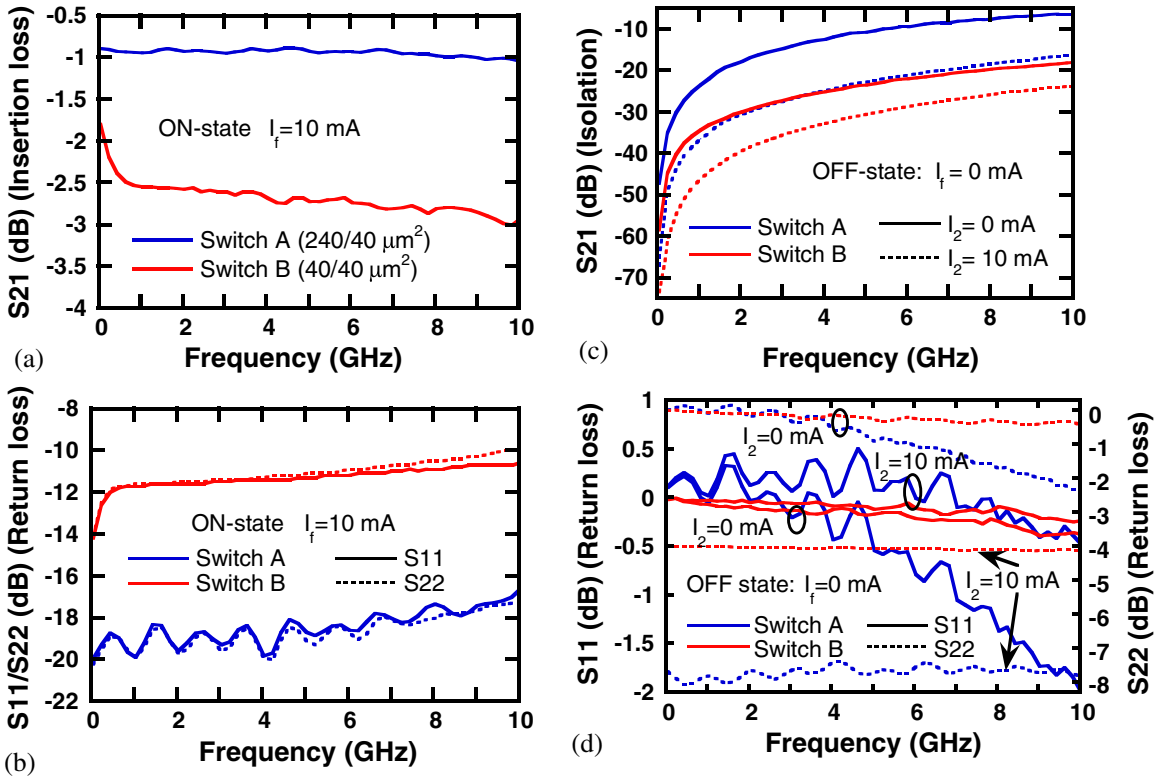

Figure 5. Measured S-parameters of two shunt-series SiNM PIN SPST switches. Switch A: D1/D2 = 240/40 μm^2. Switch B: D1/D2 = 40/40 μm^2. D1: series diode. D2: shunt diode. (*a*) S21 (insertion loss) under the ON state. D1 is biased at I_f = 10 mA. D2 is under zero bias (I_2 = 0 mA). (*b*) S11/S22 (return loss) under the ON state (with the same ON bias conditions). (*c*) S21 (isolation) under the OFF state biased at zero bias and I_2 = 10 mA. (*d*) S11/S22 (return loss) under the OFF state. (Colour online).

By comparing figures 5(*a*) and (*c*), one can easily find out that the larger is area D1, the better is the insertion loss under the ON state, however, with worse isolation under the OFF state. As a result, a compromise in the selection of the diode area for D1 will be needed in practice, which is similar to the individual series diodes, as shown in figure 4(*a*). Overall, excellent RF performance characteristics have been obtained from the RF switches when they are operating under flat (unbent) conditions. Of more importance, the microwave/RF switches are now integrated on a low-temperature flexible polymer substrate.

3.3. Switch performance under bending

Since flexible devices are likely to experience bending during operation, it is important to understand the performance characteristics of the RF switches under bending conditions. In order to perform the bending characterizations, the flexible chip was mounted on bending test fixtures with different radii, ranging from 21 to 77.5 mm. Figure 6(*a*) shows a picture of the bending test setup. Due to the relatively big size of the RF GSG probes, only convex (not concave) bending conditions can be evaluated at microwave frequencies using these probes. In order to simplify the analysis of the measurement results, the RF switches were bent along the input-to-output (port) direction, as illustrated in figure 6(*b*). Since the D1 and D2 are arranged perpendicular to each other in the switches and due to the presence of the thick (∼175 μm) PET substrates, these two diodes experience different uniaxial strain conditions under the convex bending. As shown in figure 1(*f*), and also in figures 2(*a*) and (*d*), each diode consists of two SiNM strips. Under convex bending, D1 experiences uniaxial tensile strain perpendicularly to its PIN direction (i.e. parallel to the input-to-output direction) as indicated by the left-side double arrow in figure 2(*d*). For D2, all the relevant directions are perpendicular to that of D1. Only switch B was tested under bending.

Figure 6(*c*) shows the OFF state (I_f = 0 mA) performance of the RF switch (switch B) under different bending conditions. Corresponding to the convex bending radii of 77.5 mm, 38.5 mm, 28.5 mm and 21 mm, the tensile strain values in both D1 and D2 were calculated to be ∼0.11%, 0.23%, 0.31% and 0.42%, respectively. As shown in figure 6(*c*), negligible changes in S21 were observed. Apparently, the strain has negligible effects on the resistance of D1. Since D1 also dominates S11 and S22 under the OFF state, no substantial changes in the measured S11 and S22 were observed, as shown in figure 6(*d*). Limited by measurement accuracy, no specific trend of the tiny changes can be observed for the different bending radii.

Figure 6(*e*) shows the OFF state isolation and the return loss of the switch under bending when D2 was forward biased (I_f = 0 mA, I_2 = 10 mA). Again, no substantial changes were measured for S21 due to bending. In addition, S11 stays unchanged by the bending. However, S22 was substantially improved due to the influence of the forward biased D2.

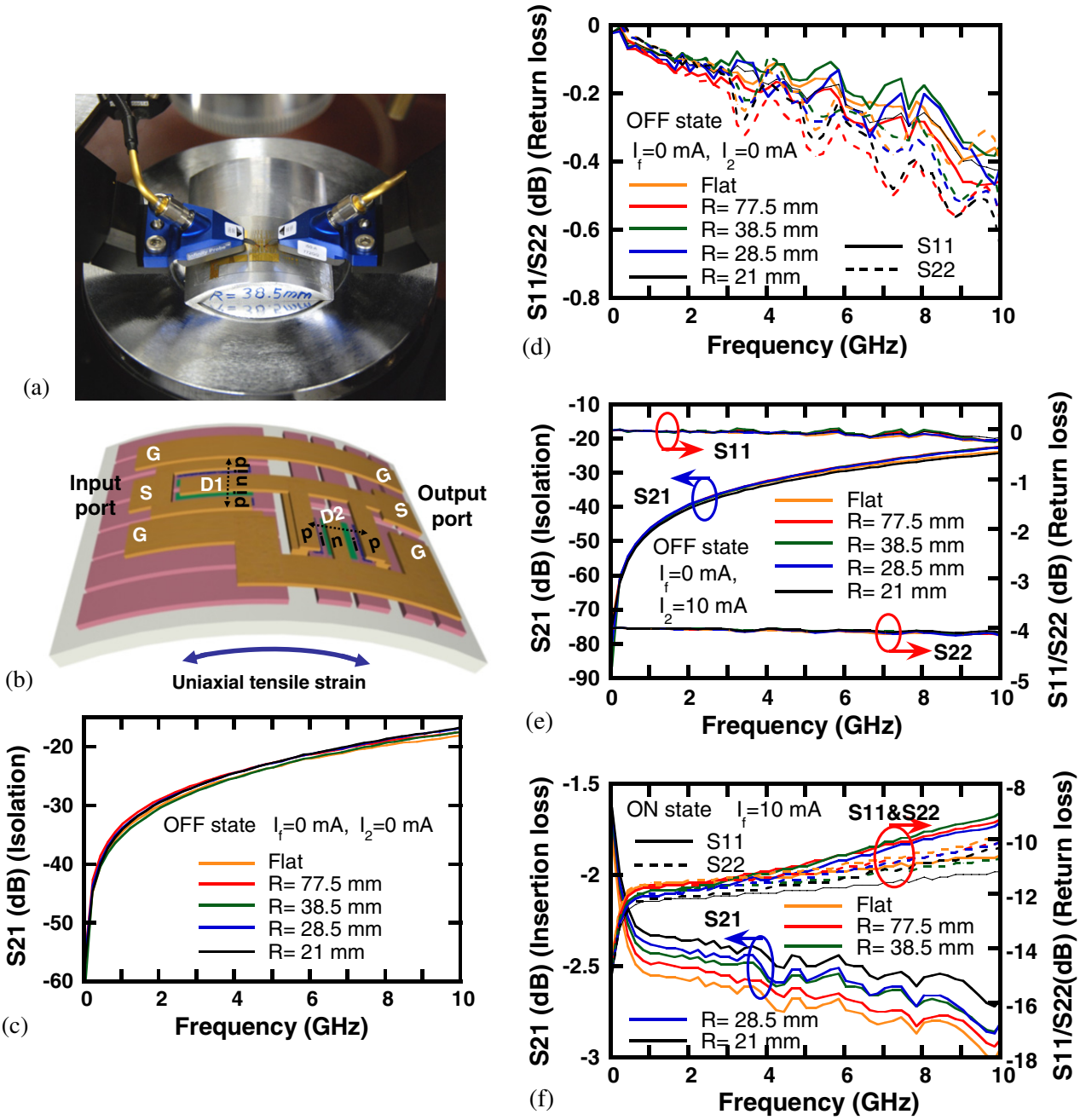

Figure 6. RF switch characterizations under uniaxial mechanical bending. (*a*) Measurement setup for the bending tests of the RF switches. (*b*) Illustration of the mechanical bending direction for the SPST PIN diode switch under bending test. The double arrows show the PIN directions of the two diodes (also refer to figure 2(*a*) for the cross-section). (*c*) Measured S21 (isolation) and (*d*) S11 and S22 (return loss) of shunt-series SiNM PIN SPST switch under the OFF state $I_f = 0$ mA, $I_2 = 0$ mA. (*e*) Measured isolation and return loss under the OFF state with bias $I_f = 0$ mA, $I_2 = 10$ mA. (*f*) Measured ON state ($I_f = 10$ mA) insertion loss and return loss of the switch. The series and shunt PIN diodes both have area of 40 μm^2. (Colour online).

Within the improved values, no strain-induced effects can be observed.

The ON-state (I_f = 10 mA, D2 zero biased) RF characteristics of the RF switch under bending were shown in figure 6(*f*). It can be seen that improved insertion loss (S21) and return loss (S11 and S22) were observed for the RF switch with the increase in tensile strain. For example, S21 improves from $\sim$−2.7 dB under flat condition to $\sim$−2.5 dB under 0.42% tensile strain at 5 GHz. Since the bending is applied along the input-to-output direction and the D1's PIN direction is arranged perpendicular to the bending direction (figure 6(*b*)), no tensile strain was applied to D1 along its PIN direction. However, tensile strain was indeed applied to the direction perpendicular to the PIN direction. Therefore, the Poisson-effect induced compressive strain was applied along the PIN direction of D1. As indicated earlier, the I-region of the diodes is lightly p-type doped. Under compressive strain, the hole mobility of the I-region has been enhanced and the PIN diode ON state resistance will thus be reduced [21]. As the strain increases, the diode resistance continues to go

down. As a result, S21 (insertion loss) has been monotonically improved with the increase in bending strain. Further bending tests were performed for the switch under the ON state with higher forward current for D1 ($I_f = 20$ mA, 30 mA), and the same improvement trend as that $I_f = 10$ mA was observed. We have applied numerous times of bending up to the smallest bending radius of our text fixture (21 mm), no degradation on the performance was observed. These bending experiment results indicate that the microwave/RF SiNM switches are robust under high mechanical deformations. The feature of mechanical flexibility of the RF switches will enable their wider application than that of their rigid counterparts fabricated in the conventional ways.

4. Conclusion

Employing flexible and transferrable single crystalline silicon nanomembranes released from SOI, a high-fidelity registration flip transfer technique and a series of high-temperature and low-temperature processes, we have demonstrated the realization of flexible PIN diode and RF switch with high performance on low-temperature plastic substrates. These RF switches can be monolithically integrated together with high-performance SiNM-based active devices on low-cost plastic substrates. The lateral SiNM PIN diodes exhibit typical rectifying characteristics with insertion loss and isolation better than 0.9 dB and 19.6 dB from DC to 5 GHz. Power handling up to 22.5 dBm without gain compression is obtained from the flexible Si PIN diode. By using shunt-series configuration of the lateral PIN diodes, a high-performance RF/microwave SPST switch is fabricated and achieves insertion loss better than 0.6 dB and isolation higher than 22.8 dB up to 5 GHz. The performance of the microwave switch under bending conditions is investigated and it shows improved performance with the application of mechanical strains. Our study further demonstrates the considerable potential for use of flexible SiNMs for high-performance flexible microwave components. Further investigations of SiNMs will lead to the realization of monolithic microwave integrated circuits and systems on low-cost flexible substrates.

Acknowledgments

This work was supported partly by the AFOSR under Grant No. FA9550-06-1-0487 and NSF MRSEC under Grant DMR0520527. The program manager at AFOSR is Dr Gernot Pomrenke.

References

[1] Reuss R H *et al* 2005 *Proc. IEEE* **93** 1239
[2] Sirringhaus H, Kawase T, Friend R H, Shimoda T, Inbasekaran M, Wu W and Woo E P *Science* **290** 2123
[3] Lu X and Xia Y 2006 *Nature Nanotechnol.* **1** 163
[4] Chen Y, Au J, Kazlas P, Ritenour A, Gate H and McCreary M 2003 *Nature* **423** 136
[5] Gelinck G H *et al* 2004 *Nature Mater.* **3** 106
[6] Baude P F, Ender D A, Haase M A, Kelley T W, Muyres D V and Theiss S D 2003 *Appl. Phys. Lett.* **82** 3964
[7] Ong B S, Wu Y and Liu P 2005 *Proc. IEEE* **93** 1412
[8] Afentakis T, Hatalis M, Voutsas A T and Hartzell J 2006 *IEEE Trans. Electron Devices* **53** 815
[9] Menard E, Lee K J, Khang D-Y, Nuzzo R G and Rogers J A 2004 *Appl. Phys. Lett.* **84** 5398
[10] Meitl M A, Zhu Z-T, Kumar V, Lee K J, Feng X, Huang Y Y, Adesida I, Nuzzo R G and Rogers J A 2006 *Nature Mater.* **5** 33
[11] Yuan H-C, Ma Z, Roberts M M, Savage D E and Lagally M G 2006 *J. Appl. Phys.* **100** 013708
[12] Ahn J-H, Kim H-S, Lee K J, Zhu Z, Menard E, Nuzzo R G and Rogers J A 2006 *IEEE Electron Device Lett.* **27** 460
[13] Yuan H-C and Ma Z 2006 *Appl. Phys. Lett.* **89** 212105
[14] Yuan H-C, Celler G K and Ma Z 2007 *J. Appl. Phys.* **102** 034501
[15] Cohen G M, Mooney P M, Paruchuri V K and Hovel H J 2005 *Appl. Phys. Lett.* **86** 251902
[16] Mack S, Meitl M A, Baca A J, Zhu Z-T and Rogers J A 2006 *Appl. Phys. Lett.* **88** 213101
[17] Yuan H-C, Qin G, Celler G K and Ma Z 2009 *Appl. Phys. Lett.* **95** 043109
[18] Sun P, Wang L, Upadhyaya P and Heo D 2005 2005 *IEEE Workshop on Microelectronics and Electron Devices (Boise, ID)* p 38
[19] Combes P F, Graffeuil J and Sautereau J-F 1987 *Microwave Components, Devices and Active Circuits* (New York: Wiley)
[20] Doherty W E and Joos R D 1993 *Microw. RF* **32** 119
[21] Uchida K, Zednik R, Lu C-H, Jagannathan H, McVittie J, McIntyre P C and Nishi Y 2004 *Int. Electron Devices Meeting (San Francisco, CA)* p 229